Journal of Marine Science and Technology

Volume 28 | Issue 1 Article 3

VERIFICATION AND VALIDATION OF A RESISTANCE MODEL FOR TANKER 17.500 DWT

D. Purnamasari
Indonesian Hydrodynamic Laboratory, Indonesia, dianpurnamasari173@yahoo.co.id

I. K. A. P. Utama
Department of Naval Architecture, Sepuluh Nopember Institute of Technology (ITS), Surabaya, Indonesia

I. K. Suastika
Department of Naval Architecture, Sepuluh Nopember Institute of Technology (ITS), Surabaya, Indonesia

VERIFICATION AND VALIDATION OF A RESISTANCE MODEL FOR TANKER 17.500 DWT

Acknowledgements

The first author expressed her gratitude to The Ministry of Research and Technology (Ristekdikti) and Higher Education of the Republic of Indonesia which funding her Ph.D. program at ITS under contract number 07/S3/D/PTB/XI/2015. The authors would like to thank the staff member of the Indonesian Hydrodynamic Laboratory and Institut Teknologi Sepuluh Nopember for their sincere support during the experiment.

Journal of Marine Science and Technology, Vol. 28, No. 1, pp. 18-24 (2020)
DOI: 10.6119/JMST.202002_28(1).0003

VERIFICATION AND VALIDATION OF A RESISTANCE MODEL FOR TANKER 17.500 DWT

D. Purnamasari[1], I. K. A. P. Utama[2], and I. K. Suastika[2]

Key words: resistance, verification and validation, numerical uncertainty.

ABSTRACT

Verification and validation study was performed based on to the methodology and procedures of the International Towing Tank Conference. The verification was based on a mesh dependency study, Richardson extrapolations, and uncertainty analysis with factor of safety methods. The validation was performed by comparing the experimental data of the 17.500 DWT tanker, tested in calm water at the Indonesian Hydrodynamic Laboratory, with computational data. The verification and validation results revealed that it was possible to improve the reliability of the numerical simulation by reducing the errors and uncertainties related to resistance prediction.

I. INTRODUCTION

Verification and validation (V&V) are essential tools for improving and interpreting numerical models of computational fluid dynamic (CFD) results. CFD results are meaningless without knowledge of their associated uncertainty. An overview of the overall V&V approach used in ship hydrodynamics has been provided, including methodology and procedures (Stern et al. 2001). A review of the CFD workshops in Gothenburg in 2010 (Larsson et al., 2010) and in Tokyo in 2015 for V&V of ship hydrodynamics revealed that the developed CFD methods achieved superior results to those of experimental methods. Larsson et al. (2014) categorized the most common verification methods into three types: grid convergence index, factor of safety (FS), and least squared root. Roache (1997) presented various approaches for error estimation and the quantification of uncertainty in CFD. Systematic grid convergence studies are the commonest, most straightforward, and arguably the most reliable technique for the quantification of numerical uncertainty. Eça and Hoekstra (2014) presented a method for estimating numerical uncertainty based on grid refinement studies and on the flow surrounding a tanker, and excellent performance is obtained for the manufactured solutions. A combination of physical and numerical modeling approaches has always been the rational strategy for research activities and commercial services. For example, the performance of the ship model KVLCC2 using detached eddy simulation with a moderate resolution of 13 million cells at 0°, 12°, and 30° drift validated the experimental data (Xing et al. 2012). In a workshop on CFD for ship hydrodynamics (Deng et.al. 2015), the total resistance for the Japan Bulk Carrier (JBC), a new ship hull used in Tokyo in 2015, was determined; the error obtained using a mesh containing a few million cells was usually less than 2% according to the explicit algebraic stress model.

Determining the accuracy and uncertainty of resistance data for both numerical and experimental methods is necessary due to the increase in CFD use in ship design and hydrodynamics research. Different procedures and standards have been developed for this purpose; some of these apply to any numerical code, whereas others are for specific applications. The various International Towing Tank Conference (ITTC) guidelines on V&V are those with codes 7.5-03-01-01, 7.5-03-01-02, 7.5-03-01-03, and 7.5-03-01-04.

The objective of this study was to conduct V&V according to the methodology and procedures prescribed in ITTC guidelines (ITTC, 2014). The verification was based on a mesh dependency study, Richardson extrapolations, and uncertainty analysis with FS method. The validation was performed by comparing CFD data with experimental data using a 17.500 DWT tanker. The experiment was conducted in calm water conditions at the Indonesian Hydrodynamic Laboratory.

II. EXPERIMENTAL PROCEDURE

1. Model Geometry

The hull form under consideration is the tanker 17.500 DWT. The main particulars are given in Table 1. This hull has a bulbous bow in the fore and stern in the aft, also a large block coefficient (C_B). The hull geometry is given in Fig. 1. The model was constructed on the 1/25 scale and made of wood. The resistance measurements were performed in a large tow

Paper submitted 04/10/9; revised 05/22/19; accepted 11/12/19. Author for correspondence:Dian Purnamasari (e-mail: dianpurnamasari173@yahoo.co.id)
[1] Indonesian Hydrodynamic Laboratory, Indonesia
[2] Department of Naval Architecture, Sepuluh Nopember Institute of Technology (ITS), Surabaya, Indonesia

Table 1. Main particulars of the tanker 17.500 DWT

Particulars	Ship	Model
Length between perpendiculars (m)	149.500	5.980
Breadth (m)	27.700	1.108
Draft (m)	7.000	0.280
Displacement volume (m^3)	23.464	0.150
Wetted surface area (m^2)	5307	8.491
Scale Ratio		1/25

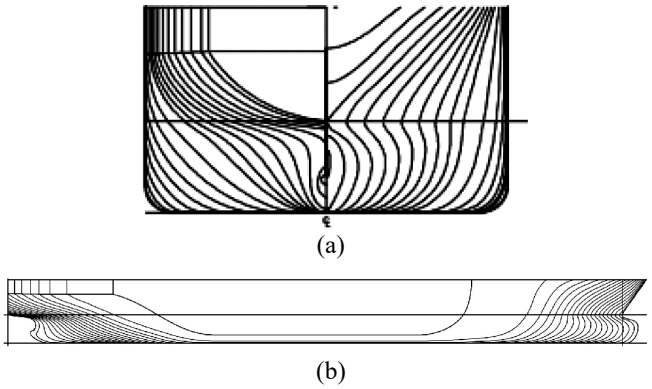

Fig. 1. Tanker 17.500 DWT hull geometry (a) Body plan (b) Side view

ing tank, which was 234.5 m long (including harbor), 11 m wide, and 5.5 m deep. The tank was equipped with a digitally controlled drive carriage and signal conditioning, and had accurate sensors installed as the data acquisition equipment. The maximum carriage speed of the towing tank was 9 m/s. The hull model was fitted to the carriage, and tests were performed using the resistance dynamometer R56 (50 kg load cell), which was manufactured based on a Kempf & Remmers design combined with a clamp serve for measuring the resistance of the model ship in the carriage (Fig. 2). Model experiments with free trim and sinkage, and restrained movements in the surge, sway, roll, and yaw were performed for further analysis. Resistance was measured at six forward speeds, corresponding to Froude numbers (*Fr*) from 0.134 to 0.201, and full-scale advance speeds from approximately 10 to 15 knots. The towing force (in kg) was converted to Newtons (N) by multiplying it with g = 9.8 m/s^2. Towing tank water temperature was measured using a digital thermometer at the model mid-draft (ITTC, 2011). The resistance values of the ship model were measured in the bare hull condition without appendages (the rudder and the propeller).

III. NUMERICAL METHOD

A model of a 17.500 DWT tanker was simulated in right-handed conditions at six different speeds from 1.029 to 1.543 m/s (corresponding to a variation from 0.134 to 0.201 in the *Fr*). The calm water resistance was computed with FINE/

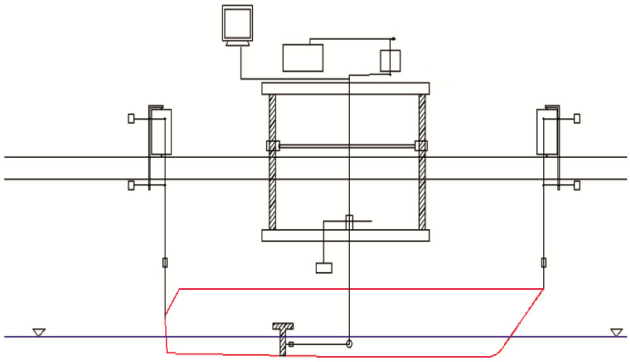

Fig. 2. Experimental setup

Marine 3.1 ISIS-CFD software to solve the incompressible Reynolds-averaged Navier Stokes (RANS) equations (Numeca, 2013). The solver applied finite volume spatial discretization. An interface capturing approach was used to model the free surface. The water-to-air interface was recovered from the volume fraction (Queutey and Visonneau, 2007). The two-equation $k\omega$-SST model (SST Menter) and turbulence model were applied in the present study (Menter, 1994), and both models provided accurate predictions for ship hydrodynamics.

The simulations were applied by importing geometrical measures to meshing, solving, and postprocessing. A parasolid format of model hull importing and the mesh was generated with an unstructured hexahedral mesh generator (Hexpress; Numeca, 2013). Hexahedral elements provide the best accuracy, and unstructured grids provide greater flexibility in the choice of cell types, thus simplifying the grid generation process for complex geometries. A computational domain was constructed by defining a box surrounding the model. A far field boundary condition was applied to the side, inlet, and outlet boundaries. A slip condition was applied to the deck. A prescribed pressure boundary condition was applied to the top and bottom boundaries (Fig. 3). A 5-step method for rapid mesh set up of complex geometries was applied. The initial mesh: in this step, the initial mesh was generated by subdividing the domain in the vertical and longitudinal directions. The subdivision for the complete domain in the vertical direction was corrected for the part above the water line. Adapt to geometry: this step comprised two successive actions, namely refinement and trimming. Refinement adapted the initial mesh such that the cell size satisfied the geometry-dependent criteria. Trimming removed the cells intersecting the geometry or those located outside the computational domain. Snap to geometry: in this step, a volumic mesh was created, which involved using sophisticated algorithms to recover lower-dimensional geometric features such as corners and curves in the mesh. Optimization: in this step, cells were fixed to increase the quality of the mesh to guarantee that all volumes were positive. The grid vertices of the mesh were

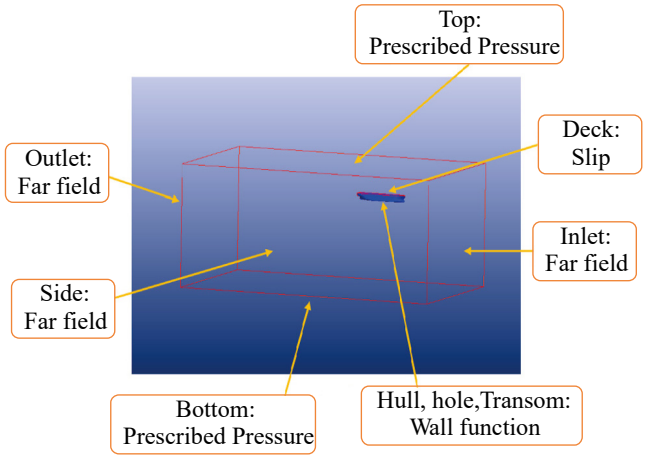

Fig. 3. Rectangular computation domain and boundary condition

repositioned based on orthogonality, aspect-ratio, and expansion-ratio criteria. Viscous layers: The viscous layer settings are first-layer thickness, growth ratio, and the number of layers. Generally, the first-layer thickness and growth ratio were the same for all surfaces.

The simulation was set up as a steady-state solution. A single-body model was defined that used all the facets of the ship's geometry. The model geometry should ensure dynamic similarity with the running condition of the ship in terms of these dimensionless numbers. The two main dimensionless parameters (Fr and Reynolds number [Re]) relevant to free surface flows surrounding a ship are defined as follows:

$$F_r = \frac{V}{\sqrt{gL_{pp}}} \tag{1}$$

$$R_e = \frac{\rho U L_{pp}}{\mu} \tag{2}$$

where Fr is Froude Number, Re is Reynolds Number, ρ is the mass density of water (kg/m^3), ν is viscosity (m^2/s), V is speed (m/s), L_{pp} is length between perpendiculars (m), and g is gravity constant (m/s^2).

The fluid properties of the model were simulated by selecting the density and viscosity of the fluid. Fluid 1 was water, with a a dynamic viscosity of 1.04362 × 10^{-3} Pa-s and a density of 996.5 kg/m^3, and Fluid 2 was air, with a dynamic viscosity of 1.85 × 10^{-5} Pa-s and a density of 1.2 kg/m^3. The general parameters of the computational control involved running computations for 1000 iterations with convergence criteria—second order and five nonlinear iterations, and the solution was saved after every 50 iterations.

The conservation of the momentum of incompressible fluid flow and the conservation of mass were described using RANS equations. They are respectively given as follows:

$$\frac{D(\rho \boldsymbol{u})}{Dt} = \nabla p + \nabla.\tau + \boldsymbol{F}_{ext} \tag{3}$$

$$\nabla.\boldsymbol{u} = 0 \tag{4}$$

where D/Dt denotes the material derivative d/dt + **u** · ∇, **u** is the velocity vector, ρ is the fluid density, p is the pressure, **F**ext is the external force vector, and $\boldsymbol{\tau}$ is the stress tensor (Ferziger and Peric, 1996).

The uncertainty analysis of results generated through RANS equations was performed according to the recommendations of ITTC. Grid studies were conducted using four grids and estimating grid errors and uncertainties using three grids (e.g., grids1-3 and grids 2-4). Convergence studies of three solutions were conducted to evaluate the convergence concerning the input parameter. Changes in the three solutions were used to define

$$R_G = \varepsilon_{G,21} / \varepsilon_{G,32} \tag{5}$$

where RG is the convergence ratio, $\varepsilon_{G,21}$ is a fine-medium error, and $\varepsilon_{G,32}$ is a medium-coarse error.

Richardson extrapolation (RE)-based methods i-th the three solutions were used to provide one-term estimates for error and order of accuracy:

$$\delta^*_{RE_G} = \frac{\varepsilon_{G,21}}{r_G^{p_G} - 1} \tag{6}$$

$$p_G = \frac{ln\left(\varepsilon_{G,32} / \varepsilon_{G,21}\right)}{ln\left(r_G\right)} \tag{7}$$

An FS approach (Roache, 1997) was used to determine the grid uncertainty of the finest mesh, wherein an error estimate from RE was multiplied by an FS to bound simulation errors as follows:

$$U_G = \left(F_s - 1\right)\left|\delta^*_{RE_G}\right| \tag{8}$$

Validation was applied to assess simulation modeling uncertainty U using the experimental data-adopted V&V 20 2009 Standard (ASME 2009). Therefore, the numerical uncertainty U_{SN} was equal to the grid uncertainty U_G (Stern et al., 2001). The validation uncertainty is calculated as:

$$U_V^2 = U_D^2 + U_G^2 \tag{9}$$

where U_D is the uncertainty of model test.

IV. RESULT AND DISCUSSION

On the basis of changes in initial cell sizes, grid independence studies were conducted (Table 2), and three volumic

Table 2. Number of cells for the mesh dependency study

	Initial mesh			Number of Cells
	x	y	z	
Coarse	10	6	4	807.952
Medium	15	9	6	1.487.007
Fine	20	12	8	2.513.477
Finest	25	15	10	5.121.534

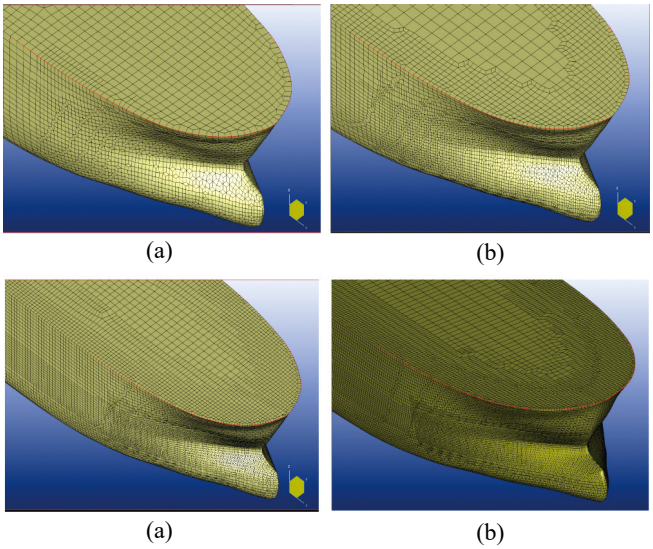

Fig.4. The complete generated mesh (a) coarse (b) medium (c) fine (d) finest

refinement boxes were added to the initial mesh. Different initial meshes lead to different mesh sizes, allowing refinement of the whole fluid volume, and not only of the areas adjacent to the solid components. The completely generated coarse, medium, fine, and finest meshes are presented in Fig. 4, comprising approximately 800,000 to 5.1 million cells with a design speed Fr = 0, 175. The selected wall distance for the generated meshes was y^+ = 30. Hence, the wall function was implemented in the boundary conditions of the ship, and viscous prismatic cells surrounding the hull comprised 20 layers with an expansion ratio of 1.2.

All refinements were applied relative to the initial mesh size. Fig. 5 presents the generated fine mesh, which surrounds the free surface location. Further refinement was applied to the mesh based on the shape of the internal surface. All created grids had a satisfactory quality, which did not influence the stability and computation result. Mesh quality was essential for controlling discretization errors. Important measures of mesh quality may be categorized as measures of mesh orthogonality, expansion ratio, and aspect ratio (or stretching). The acceptable values mesh orthogonality, expansion-ratio, and aspect-ratio were >20°, <20, and <100, respectively (Fig. 6).

Wave patterns surrounding the hull and centerline symmetry plane for a design speed 13 knots are presented in Fig. 7. To

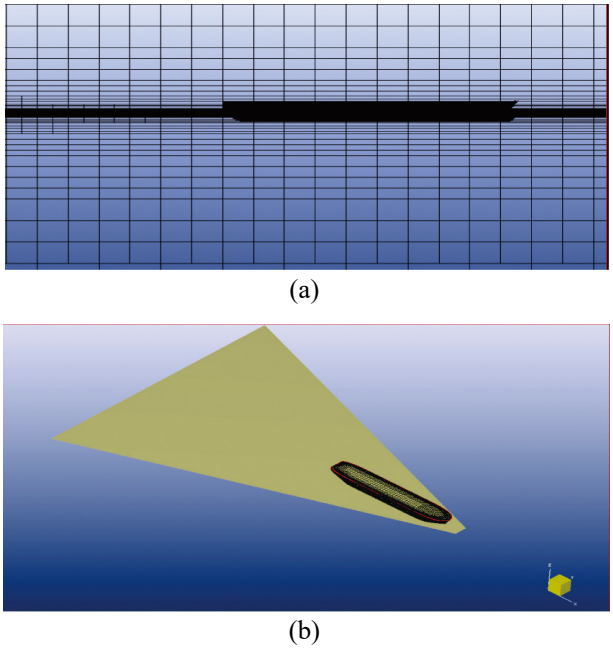

Fig.5 (a) Mesh around the free surface (b) mesh internal surface

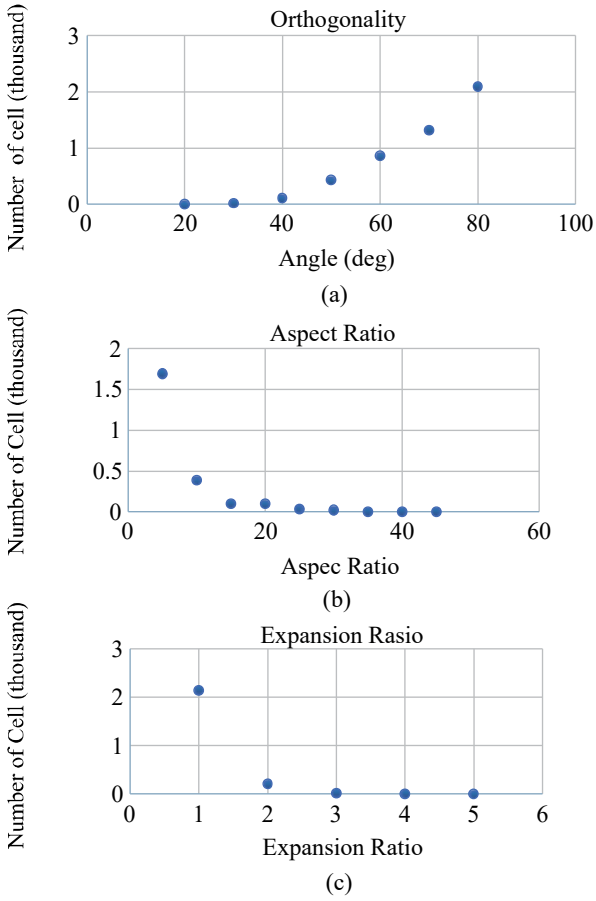

Fig. 6. Mesh quality check (a) orthogonality (b) aspect ratio (c) expansion ratio

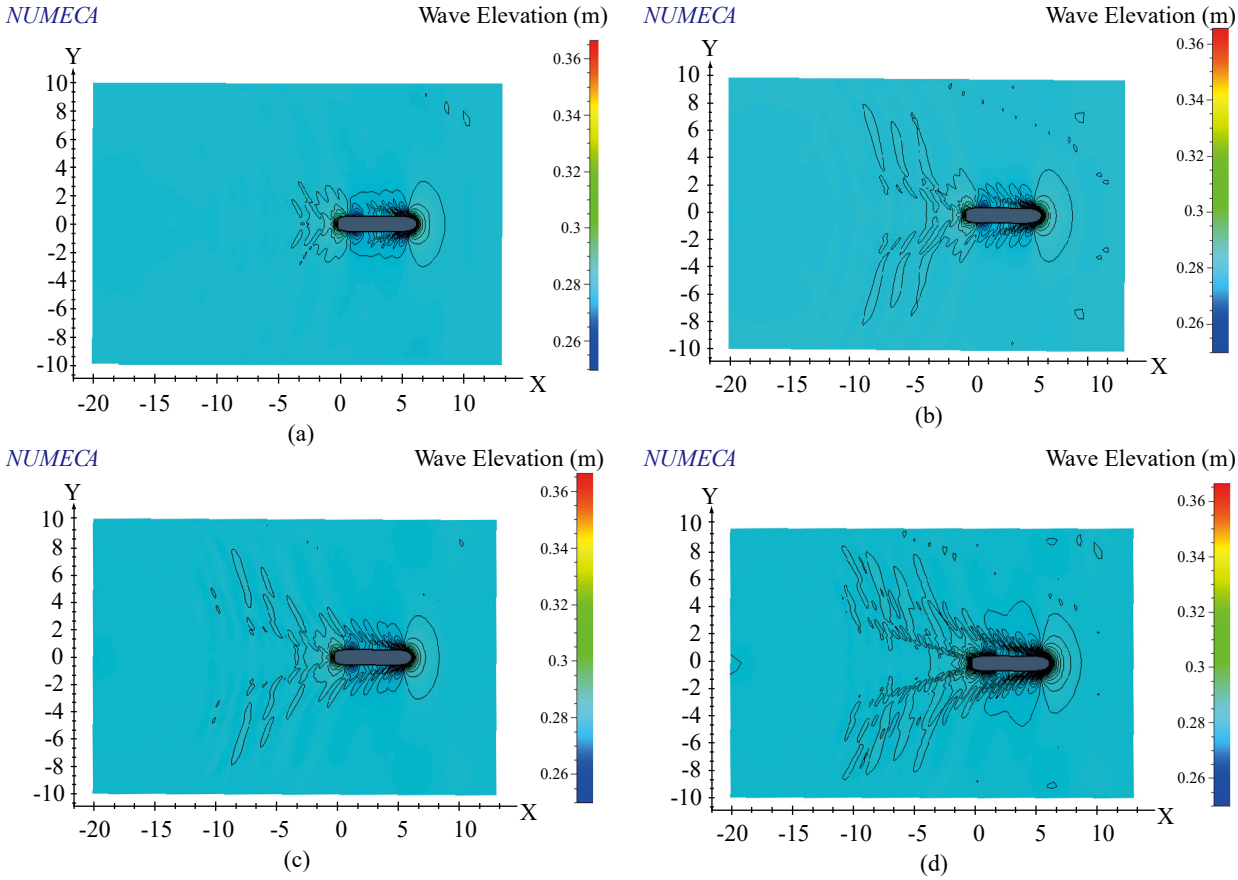

Fig. 7. Wave patern around model ship (a) grid coarse (b) grid medium (c) grid fine (d) grid finest

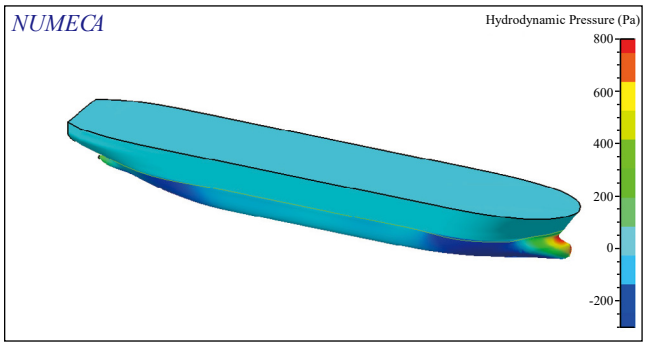

Fig. 8. Hydrodynamic Pressure

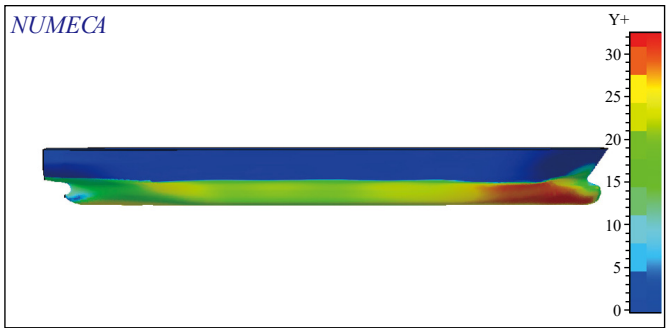

Fig. 9. Wall Y^+ distribution on the hull surface

properly capture the change in the wave pattern, refinement of the three meshes or discretization of the statically finer mesh near the free surface was performed at *Fr 0.175*. The wave pattern generated by the hull in calm water is a crucial factor that affects ship resistance. In addition, the waveform symmetry in the flow field of the hull can be an indicator of whether the computation is correct. The contour plots of hydrodynamic pressure acting on the hull surface are presented in Fig. 8. The colors on the hull indicate pressure levels; blue indicates low pressure and red indicates high pressure. Higher pressure was noted near the bow.

Regarding wall functions, the first point from the wall was well within the logarithmic layer of the boundary layer. Therefore, ay^+ of 30 was recommended (ITTC, 2014). The recommended acceptable ranges were $30 < y^+ < 100$ (Fig. 9).The pressure distribution under the model hull and free surface can be observed in Fig. 10.

Table 3 lists the numerical results obtained from three meshes. The results indicate that the finest mesh predicts the total resistance with higher accuracy than the other meshes. as described by Purnamasari et al., 2018.

Table 3. Grid convergence study for total C_T (10^3)

Fr	Coarse	Medium	Fine	Finest	Exp
0.134	4.34	4.26	4.21	4.14	4.18
0.148	4.35	4.24	4.12	4.10	4.09
0.161	4.29	4.22	4.17	4.15	4.24
0.175	4.39	4.35	4.26	4.17	4.15
0.188	4.36	4.28	4.20	4.22	4.29
0.201	4.87	4.79	4.69	4.57	4.59

Table 4. V&V result

R_G	P_G	U_G	U_D	U_{val}
0.59	1.3	1.1%	0.77%	1.4%
0.68	1.4	1.6%	0.82%	2.1%
0.74	2.1	1.4%	0.86%	2.2%
0.60	1.6	1.9%	0.79%	2.6%
0.52	2.1	2.9%	0.97%	3.1%
0.64	2.2	2.2%	1.12%	2.9%

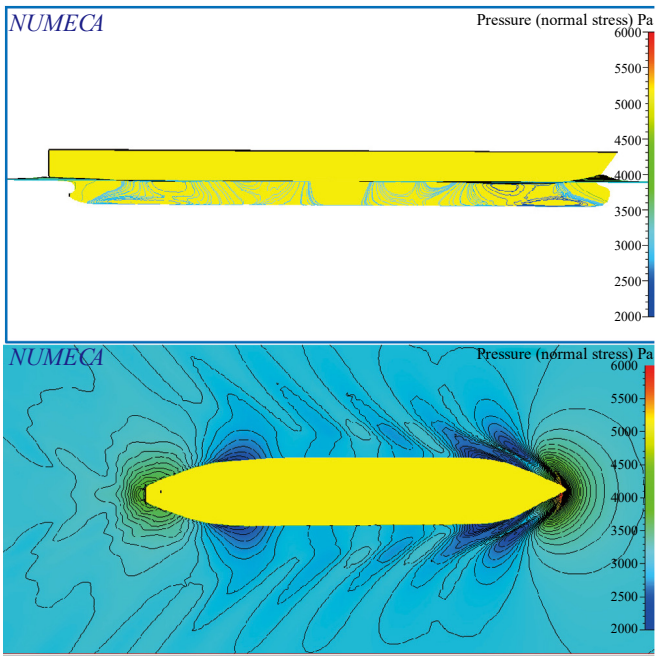

Fig. 10. Pressure distribution

Fig. 11 presents the total resistance of the model due to the different grid sizes at *Fr* 0.175. On increasing the number of elements to more than 5.1 M, the total resistance converged with the increase in grid size. V&V results are presented in Table 4. The convergence condition corresponds to three solutions, as the monotonic convergence was achieved with R of <1. Every three grids adopted the same refinement ratio $r_G = \sqrt{2}$. The validation uncertainty for the finest grid for all *Fr* values was <4%.

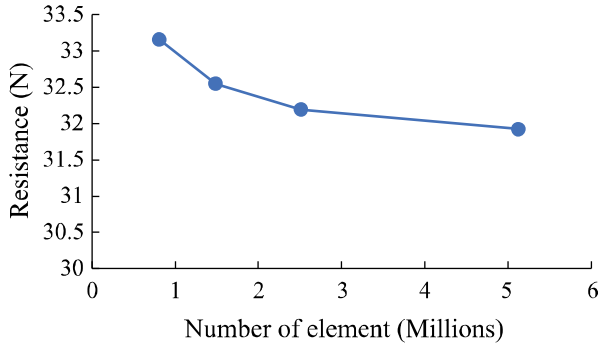

Fig. 11. Relation between number of elements and resistance results

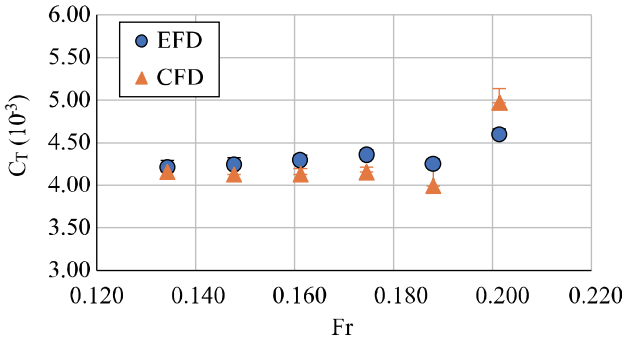

Fig. 12. Results for total resistance coeffcient C_T

Fig. 12 presents the comparison of results of Experimental Fluid Dynamics (EFDs; the experimental data) and CFDs (simulation data) for the total resistance coefficient CT. Numerical uncertainty was relatively minor when using the FS method, which it was generally less for small *Fr* values. However, when *Fr* was large, FS was slightly higher than the data uncertainty. Such a trend was expected because of the boundary layer condition, and the free surface resolution of the grids was optimal for the designed *Fr* (13 knots), thus making the grids unsuitable for larger *Fr values*. The comparison between the experimental and steady-state simulations data revealed adequate agreement for resistance. The highest relative deviation for the fine mesh was 1.9% for a design speed of 13 knots. Fig. 13 details the wave elevation surrounding the hull in EFDs and CFDs, showing that they have a similar wave elevation. The arrows in the figure indicate that the wave elevation from simulation agrees well with that obtained from the experiment is good agreement. The analysis revealed that the numerical model was reliable and reasonable.

V. CONCLUSIONS

CFD results were approximations and not exact solutions. Thus, they were meaningless without the knowledge of associated uncertainty. The grid quality of the mesh determined the accuracy of resistance results.

The CFD result for the finest mesh was close to the exper

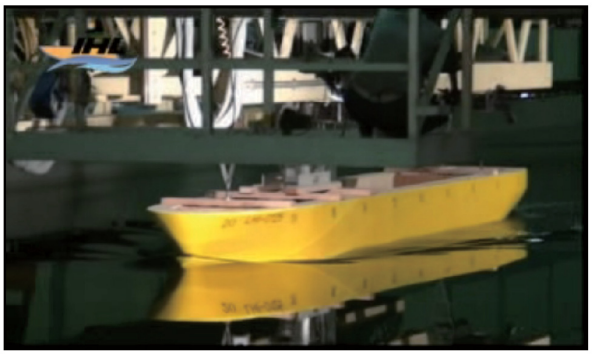

(a)

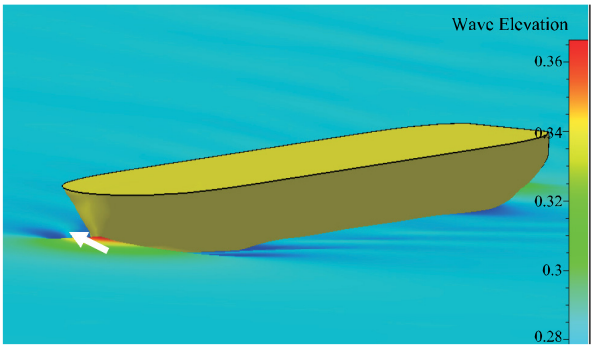

(b)

Fig. 13. Photographs between the experiment and the numerical calculations

imental result. The numerical V&V of resistance for the model hull was performed based on grid refinement studies and numerical uncertainties. The uncertainty was less than 4%. Improving the mesh resolution resulted in improved resistance prediction accuracy.

This is a valuable test case for future studies because of the agreement between the CFD computational data and experimental data for numerical V&V of ship hydrodynamics.

ACKNOWLEDGEMENT

The first author expressed her gratitude to The Ministry of Research and Technology (Ristekdikti) and Higher Education of the Republic of Indonesia which funding her Ph.D. program at ITS under contract number 07/S3/D/PTB/XI/2015. The authors would like to thank the staff member of the Indonesian Hydrodynamic Laboratory and Institut Teknologi Sepuluh Nopember for their sincere support during the experiment.

REFERENCES

ASME V&V 20. (2009). Guide on Verification and Validation in Computational Fluid Dynamics and Heat Transfer.

Deng, G., A. Leroyer, E. Guilmineau, P. Queutey, M. Visonneau and J. Wackers (2015). Verification and validation of resistance and propulsion computation. Workshop on CFD in Ship Hydrodynamics. Chalmers, Tokyo, 261-266.

Eca, L. and M. Hoekstra (2014). A procedure for the estimation of the numerical uncertainty of CFD calculations based on grid refinement studies. Journal of Computational Physics 262, 104-130.

Ferziger, J. and M. Peric (2010). Computational Methods for Fluid Dynamics, Springer (3rd Ed.)

Stern, F. R., V. Wilson, H. W. Coleman and E. G. Paterson (2001). Comprehensive approach to verification and validation of CFD simulations - Part 1: methodology and procedures. Journal of Fluids Engineering 123, 793-802.

ITTC. (2008). Uncertainty analysis in CFD verification and validation. Methodology and Procedures, No. 7.5-03-01-01.

ITTC. (2011). The Specialist Committee on Computational Fluid Dynamics. Proceedings of 26th International Towing Tank Conference, volume II, pages 337-377, Rio de Janeiro, Brazil.

ITTC. (2014). Practical Guidelines for Ship Resistance CFD. 7.5-03-02-04.

Larsson, L., F. Stern and M. Visonneau (2010). A Workshop on Numerical Ship Hydrodynamics. Report, Chalmers University of Technology.

Larsson, L., F. Stern and M. Visonneau (2014). Numerical Ship Hydrodynamics: An Assessment of the Gothenburg 2010 Workshop. Springer Verlag, Germany.

Numeca (2013). Manual Hexpress.

NUMECA (2013). Theoretical Manual FINEMarine v3.1.

Menter, F. R. (1994). Two-equation eddy-viscosity turbulence models for engineering applications. AIAA J. 32(8), 1598-1605.

Purnamasari, D., I. K. A. P. Utama, I. K. Suastika (2018). An investigation into The Numerical Uncertainty resistance model tanker 17.500 DWT. Proceeding 11th International Conferenceon Marine Technology. 13-14 August 2018, Kuala Lumpur, Malaysia. p 8-16.

Queutey, P. and M. Visonneau (2007). An interface capturing method for free-surface hydrodynamic flows. Computers & Fluids 36(9), 1481-1510.

Roache, P. J. (1997). Verification and Validation in Computational Science and Engineering, Hermosa publishers, Albuquerque, New Mexico.

Tokyo (2015). Workshop. http://www.t2015.nmri.go.jp/

Xing, T., S. Bhushan and F. Stern (2012). Vortical and Turbulent Structures for KVLCC2 at Drift Angle 0, 12, and 30 Degrees. Ocean Engineering.